CrystEngComm

Accepted Manuscript

ROYAL SOCIETY OF CHEMISTRY

www.rsc.org/crystengcomm

Facile control of inter-crystalline porosity in the synthesis of size-controlled mesoporous MFI zeolites via in-situ converting silica gel into zeolite nanocrystals for catalytic cracking

Wenlong Li, Tong Ma, Yafei Zhang, Yanjun Gong, Zhijie Wu* and Tao Dou *

[a] *State Key Laboratory of Heavy Oil Processing, Key Laboratory of Catalysis of CNPC, China University of Petroleum, Beijing, 102249, China. E-mail: zhijiewu@cup.edu.cn; doutao@cup.edu.cn.*

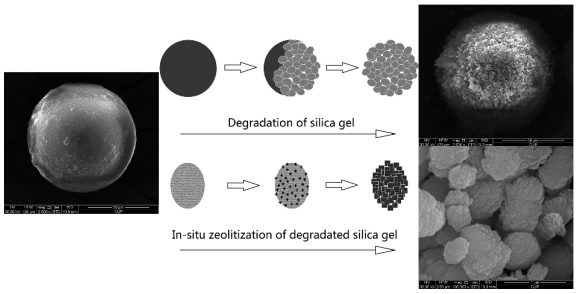

We proposed a general strategy for the green synthesis of MFI zeolite nanocrystals with controllable inter-crystalline mesopores.

Cite this: DOI: 10.1039/x0xx00000x

Received 00th January 2012,
Accepted 00th January 2012

DOI: 10.1039/x0xx00000x

www.rsc.org/

Facile control of inter-crystalline porosity in the synthesis of size-controlled mesoporous MFI zeolites via in-situ converting silica gel into zeolite nanocrystals for catalytic cracking

Wenlong Li, Tong Ma, Yafei Zhang, Yanjun Gong, Zhijie Wu* and Tao Dou*

We report here a strategy of the facile synthesis of hierarchical MFI zeolite nanocrystals with controllable inter-crystalline mesopores by one-step hydrothermal synthesis method using silica gel as the silica source and tetrapropyl ammonium as the microporous template without any other mesoporous templates or zeolite seeds. The powder X-ray diffraction results show the MFI structure with high crystallinity for all as-prepared zeolites. The scanning electron microscope characterizations show that 400-1000 nm zeolite aggregates are composed by the assembly of ~100 nm zeolite nanocrystals. The transmission electron microscope results indicate the formation of inter-crystalline mesopores in the aggregated nanocrystals among the interspace of zeolite nanocrystals. High mesopore volume (0.13 cm^3/g) and external surface area (93 cm^2/g) of the aggregated MFI zeolites are observed in N_2 sorption. The inter-crystalline porosity of MFI zeolites varies with the change of the aggregation and the size of zeolite nanocrystals by changing the sodium concentration or the types of sodium salts in aluminate-silicate gels during hydrothermal crystallization. The mesoporous MFI zeolite aggregates exhibit similar light olefin selectivities and remarkably enhanced lifetime in the catalytic cracking of hexane compared to the highly dispersed MFI zeolite nanocrystals.

Key Word: MFI zeolite, ZSM-5, Hydrothermal crystallization, Hierarchical zeolite, Catalytic cracking

1. Introduction

MFI zeolite, especially ZSM-5 zeolite, is one of the crystalline microporous materials with high thermal and acid stability, reactivity, and shape selectivity in many reactions, such as the catalytic cracking, isomerization, aromatization and alkylation. [1-6] However, the crystal size of the conventional ZSM-5 zeolite is very large (1-10 μm) compared to its micropores (10 membered-ring aperture, 0.55 nm) possessing a molecular-sieving effect. The shape selective reaction apparently is limited by the diffusion of reactant molecules within the zeolite crystals, leading to low product selectivity and fast deactivation. [6-8] In addition, since effective active sites (acidic sites) for catalytic reactions are distributed on the internal surfaces of the main channels and on the external surfaces of the crystal, the pore mouths are plugged easily because of coke deposition leading to short catalyst lifetimes.[1] Two primary strategies of faster mass transfer for avoiding these serious problems are frequently reported: the formation of intra-crystalline mesopores in zeolites and the preparation of zeolite nanocrystals generating inter-crystalline mesopores.

The intra-crystalline mesopores can be obtained by the post-treatment of zeolites, such as dealumination or desilication, [9-11] which inevitably destroys the zeolite framework and decreases the zeolite crystallinity. Also, some residues within zeolite channels may occur during post-treatments leading to the clog of micropores. Moreover, the intra-crystalline mesopores can also be designed and prepared by a dual templating method using micropore-directing agents (microporous templates) and mesopore-directing agents (mesoporous templates) in the hydrothermal synthesis, such as nanometer-sized carbon particles, carbon and polymer aerogel, cationic polymer. [12-15] However, the latter strategy is rather expensive for the industrial application.

On the other hand, the catalytic performance of many heterogeneous catalytic reactions is proven to be promoted by using zeolite nanocrystal, [16] because the diffusion path length (crystal size) for reactants decreases, and the external surface area of zeolite crystal increases resulting in more exposed acidic sites. However, the practical use of these zeolite nanocrystals (<200 nm) is rarely reported because of the difficulty in developing an economic separating method in their production and application.

Recently, the aggregates of zeolite nanocrystals with large secondary inter-crystalline mesopores have garnered increasing attention. [17-19] They retain the advantages of zeolite nanocrystals such as the reduced diffusion limitation, increased external surface area and large mesopore volume, while also show promotion in the facile separation because of their larger secondary particle sizes. Thereby, the aggregates of zeolite nanocrystals with large inter-crystalline mesopores are regarded as the promising catalytic materials in the reactions involving diffusion limitation of reactants and/or products, such as the isomerisation, cracking and methanol-to-hydrocarbons

reactions requiring high selectivity and excellent catalyst lifetime. [20]

Serrano et al. synthesized the aggregates of ZSM-5 nanocrystals with the organosilane-based method, [21] which included the pre-crystallization of raw gel, the silanization of zeolite seed and the crystallization of zeolite. However, the whole synthesis process requires 6 days or more time, and the organosilanes are expensive for industrial production. Also, the steam-assisted conversion method is frequently used in the synthesis of the aggregates of zeolite nanocrystals. [22, 23] However, the requirement of the preparation of precursor gel extends time for zeolite synthesis.

Here we present a general strategy for the green and facile production of zeolite catalysts. Hierarchical aggregates of mesoporous ZSM-5 zeolite nanocrystals were obtained by a one-step hydrothermal crystallization method by using tetrapropyl ammonium (TPA) as microporous templates. A high solid/liquid ratio (low content of water as solvent) in the hydrothermal synthesis was introduced without any other mesoporous templates or zeolite seeds. The high solid/liquid ratio possesses many advantages of reducing waste production and increasing zeolite yield, as well as eliminating high pressure. Again, the present strategy is simple and energy saving without pre-crystallization/pre-seeding step or steam-assisted conversion and with short crystallization time (<7h). Meanwhile, common and cheap silica gel was utilized as the silica source. The as-prepared ZSM-5 zeolites show better stability than conventional ZSM-5 nanocrystal in the catalytic cracking of n-hexane into light olefins.

2. Experimental Sections

2.1 Chemicals

Tetrapropyl ammonium hydroxide（TPAOH, 25 wt.% in water ）used as the microporous template for zeolites, and aluminium isopropoxide (AIP, 24 wt.% Al_2O_3) were purchased from Aldrich. Silica gel (100-200 mesh, 99 wt.% SiO_2, and stacking density > 0.4g/cm^3) was purchased from Qingdao Haiyang Chemical Co. and used as the silica source. Sodium sulfate (99 wt.% Na_2SO_4), sodium chloride(99 wt.% NaCl) and sodium hydroxide (99 wt.% NaOH) were purchased from Sinopharm Chemical Reagent Co., Ltd. Sodium carbonate (99 wt.% Na_2CO_3) and sodium Bromide(99 wt.% NaBr) were purchased from Tianjin Guangfu Technology Development Co., Ltd. All reactants were received and used without further purification.

2.2 Zeolite Preparation

The zeolite was prepared by a simple and rapid one-step hydrothermal synthesis with a high solid/liquid ratio. Neither long-time aging nor pre-crystallization/pre-seeding step was required. No mesoporous templates or zeolite seeds were used in the synthesis. Silica gel was used as the silica source.

In a typical synthesis procedure, 0.68 g of AIP was dissolved in a solution of 28.0 g of TPAOH and 6.0 g of distilled water at room temperature for 20 min, then 1.36 g of sodium bromide was added to the solution under vigorous stirring at room temperature for 20 min to obtain a homogeneously mixture solution. Subsequently, 10.0 g of porous silica gel was added into the solution under vigorous stirring. The resulting mixture was stirred further at room temperature for 1 h and then distributed in a 100 mL stainless steel autoclaves with Teflon liners. The autoclaves were put in an oven at 443 K under static conditions for 7 h. Then autoclaves were removed from the oven and quenched with water, and the solid product was collected by filtration. Finally, the product was dried at 373 K overnight and then calcined in air at 823 K for 6 h to remove the organic template.

2.3 Characterizations

The pH value was measured by a pH meter (PHS-3C, Shanghai REX Instrument Factory, China). Powder X-ray diffraction (XRD) patterns were collected on a Bruker D8 Advance diffractometer, using Cu Kα radiation (40 kV, 40 mA). The morphology and crystal size of the synthesized zeolites was observed on an FEI Quanta 200F scanning electron microscope (SEM). For transmission electron microscope (TEM) investigations, samples were suspended in ethanol under ultrasonic treatment (10 min) and dropped on a copper grid with Lacey carbon support film. The TEM images were taken using a JEM 2100 at 200 kV. The laser particle size analysis was achieved on a Malvern Mastersizer 2000.

The textural properties of the calcined samples were obtained by N_2-sorption at 77 K. Prior to the actual measurements, all samples were pre-treated under high vacuum at 573 K for 12 h. The measurements were performed on a Micromeritics ASAP 2020. The specific surface area was obtained by using the Brunauer-Emmett-Teller (BET) equation at relative pressure P/P_0 values below 0.2. Pore size distribution was obtained by using the BJH method for N_2 at 77 K with the silica desorption branch kernel based on a cylindrical pore model, and the total pore volume was estimated at P/P_0 of 0.99.

The amount of coke deposits was determined by a Mettler Toledo TGA/DSC 1. In a typical measurement, approximately 25 mg of catalysts was loaded and the thermo-gravimetric (TG) curve was recorded as the catalyst was heated from 298K to 1173K at a constant rate of 10 K/min under flowing oxygen (50 ml/min). The sample weight loss occurring above 673 K was taken as the total coke content.

Temperature-programmed desorption of ammonia (NH_3-TPD) was carried out to check the acidity of acidic sites. Prior to the measurements, about 100 mg of sample (0.38 to 0.83 mm) was degassed at 873 K for 2 h. After cooling to 373 K, the sample was saturated in NH_3 stream for 30 min, followed by purging with nitrogen for 1 h to remove co-adsorbed NH_3. The remaining strongly adsorbed NH_3 was then desorbed by heating the sample to 873K at a constant rate of 10 K/min, and the TPD signal was monitored by the thermal conductivity detector (TCD) simultaneously.

2.4 Catalytic Reaction

The calcined sodium form zeolite samples (Na-ZSM-5) were ion-exchanged three times in 1 mol/L NH_4Cl solution at 360K for 2 h, converting the Na-ZSM-5 into NH_4-form zeolites (NH_4-ZSM-5). After the ion-exchange, the zeolite samples were washed with deionized water, dried at 380K, and then calcined under static air at 823K (2 K/min ramping rate) for 6 h to obtain H-form zeolites (H-ZSM-5). Before conducting catalytic tests, the H-ZSM-5 zeolites were pelletized and sieved to retain aggregates 0.38 to 0.83 mm in diameter.

The catalytic cracking reaction was conducted in a fixed-bed reactor under atmospheric pressure. For each test, 0.5 g H-ZSM-5 catalyst was loaded in a quartz tube reactor with an inner diameter of 9 mm. Prior to catalytic activity test, the sample was activated in situ at 930 K (10 K/min ramping rate) under N_2 flow (60 ml/min) for 2 h. After the heating treatment, the sample was cooled naturally to 900 K, and then hexane was pumped through a double plunger pump by passing N_2 (P_{feed}=16 kPa) at a weight hourly space velocity (WHSV) of 8 h^{-1}.

The products were analyzed on-line by a gas chromatograph (Agilent GC7890), equipped with a 30 m capillary column (HP-PLOT Q) and a flame ionization detector (FID). The hexane conversion and hydrocarbon product selectivities were calculated as given below.

$$X_{n-hexane} = \frac{n_{n-hexane,0} - n_{n-hexane}}{n_{n-hexane,0}} \times 100\%$$

$$S_{CxHy,product} = \frac{x \times n_{CxHy,product}}{6 \times (n_{n-hexane,0} - n_{n-hexane})} \times 100\%$$

$n_{n\text{-}hexane,0}$ is the initial molar amount of hexane, $n_{n\text{-}hexane}$ is the molar amount of hexane in product; $n_{CxHy,\ product}$ is the molar amount of the product with x carbon atoms and y hydrogen atoms.

Blank experiments without H-ZSM-5 zeolites showed 13.4% conversion of n-hexane, suggesting the occurrence of thermal cracking at 900 K.

3. Results and Discussion

3.1 Structural and Textural Characterizations

A series of zeolites with different molar composition of aluminate-silicate gel (1 AIP: 50 SiO_2: 450 H_2O: 10 TPAOH: x NaBr, x = 2, 4, 6, 9, 12, respectively) were synthesized and denoted as ZSM-5_{xNa} (x= 2, 4, 6, 9, 12, respectively). The pH of the solution increases from 14.1 to 14.4 as the NaBr concentration increases. The X-ray diffraction patterns of these samples (Fig.1) show all the samples possess a series of characteristic diffraction peaks at 2θ of 7.9, 8.8, 14.8, 23.2, 23.9, 24.4 ^{o} corresponding to the structure of MFI zeolite topology (JCPDS No.: 49-0657). No other impurity can be observed in these patterns. Moreover, the high intensity of diffraction peaks indicates high crystallinity of all the as-prepared zeolites. The diffraction peaks around 2θ of 23 to 25^o become broader on the ZSM-5_{2Na} and ZSM-5_{4Na} than that on ZSM-5_{6Na} samples. These indicate the decrease of the zeolite crystal sizes proven by SEM and TEM characterization (see next sections following). These results show a high NaBr concentration in zeolite synthesis gel results in an increase of zeolite crystal size.

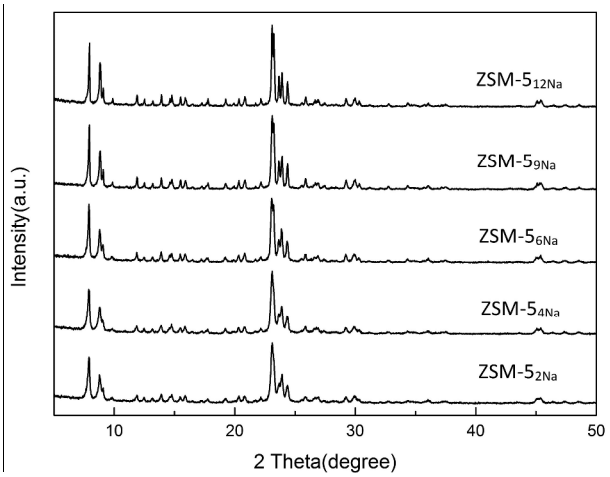

Fig.1. XRD patterns of the ZSM-$5_{x\text{-}Na}$ (x=2, 4, 6, 9, and 12) samples.

Fig.2 shows the SEM images of calcined ZSM-5 samples prepared with different NaBr concentrations in zeolite synthesis gels. Obviously, the morphology of zeolites is affected by the NaBr concentrations: the primary particle size of zeolite crystal increases with the growth of NaBr concentrations. ZSM-5_{2Na} sample exhibits primary particles of cuboid morphology below 100 nm; while ZSM-5_{4Na} sample shows primary particles of smooth edge cuboid morphology with 50 – 150 nm. Both of them possess secondary aggregates of irregular morphology with 400–1000 nm, which are assembled by many primary small nanocrystals. The size distribution of secondary aggregates on ZSM-5_{2Na} and ZSM-5_{4Na} is random, but these aggregates could be facilely collected after hydrothermal synthesis by vacuum filtering within 30 min. Unlike ZSM-5_{2Na} and ZSM-5_{4Na}, ZSM-5_{6Na} sample possesses highly dispersed nanocrystals of ellipsoid/cuboid morphology with 150-300 nm. However, the collection of ZSM-5_{6Na} from hydrothermal products requires more than 7 h using the same filtering treatment as ZSM-5_{2Na} and ZSM-5_{4Na}. Usually, the highly dispersed ZSM-5 nanocrystal like ZSM-5_{6Na} can be retrieved from high angular speed centrifugation, which makes it difficult for the industrial mass production. ZSM-5_{9Na} sample exhibits dispersed sub-micrometer crystals of common coffin morphology with 400-700 nm and ZSM-5_{12Na} sample shows large crystals of irregular morphology more than 5 μm. These data together show that the formation of ZSM-5 zeolite nanocrystals requires relatively low NaBr concentration; while the preparation of large ZSM-5 crystals (ZSM-5_{9Na}) with the similar size as conventional MFI zeolites could be achieved with a high NaBr concentration in our synthesis strategy.

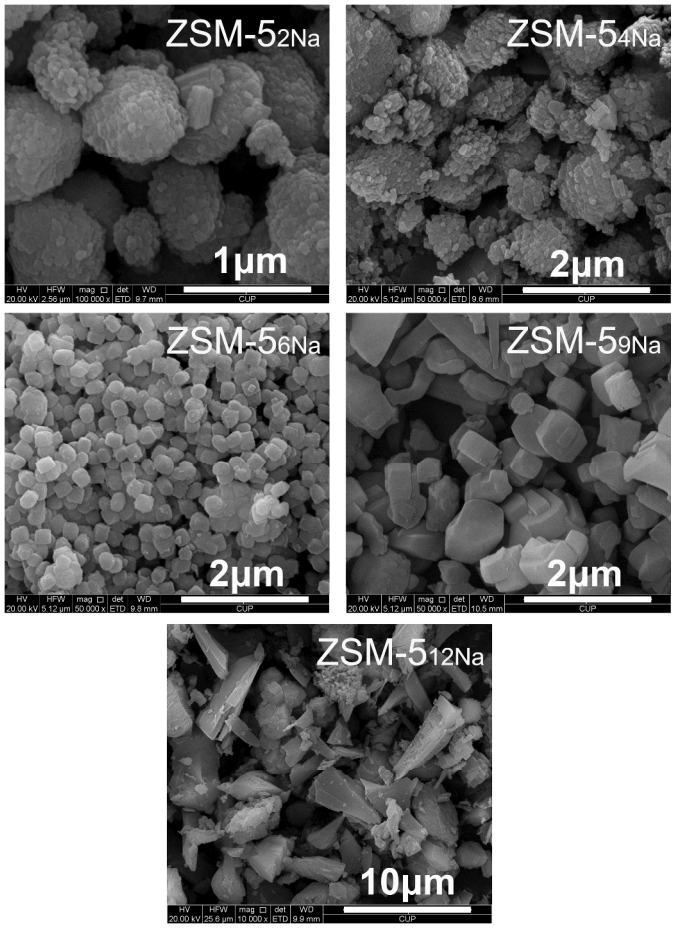

Fig.2 SEM images of ZSM-$5_{x\text{-}Na}$ (x=2, 4, 6, 9, and 12) samples.

TEM (Fig.3) and N_2-sorption (Fig.4 and Table 1) characterizations were used to probe the porosity and the textural properties of ZSM-5_{2Na}, ZSM-5_{4Na} and ZSM-5_{6Na}. The TEM images (Fig. 3a, 3c and 3e) indicate the primary particle size of MFI zeolites increases as the NaBr concentration increases in agreement with the SEM results. The HRTEM images (Fig. 3b, 3d and 3f) show a regular morphology and lattice fringes of ZSM-5 crystal for all the samples, suggesting the high crystallinity and purity of MFI zeolites. ZSM-5_{2Na} and ZSM-5_{4Na} exhibit irregular aggregates with a size of 400–1000 nm, which are formed by the assembly of lots of nanocrystals (Fig.3a and 3c). ZSM-5_{2Na} sample with a primary particle of cuboid shape with size of 40–100 nm densely aggregates, while the nanocrystals of ZSM-5_{4Na} sample with a primary particle of smooth edge cuboid shape and with size of 60–140 nm loosely aggregates, which show good consistency with SEM result. ZSM-5_{6Na} shows highly dispersed nanocrystals with a particle size of 200–300nm , suggesting the formation of inter-crystalline mesopores via the agglomeration of dispersed crystals (Table 1). The inter-crystalline mesopores among primary particles of zeolite nanocrystals become clearer on ZSM-5_{4Na} than on ZSM-5_{2Na} (Fig.3a and Fig.3c) because of the loosely aggregated nanocrystals of ZSM-5_{4Na} sample. Unlike the agglomeration of dispersed ZSM-5_{6Na} nanocrystals (Fig.3e), the aggregates of ZSM-5_{4Na} nanocrystals (Fig.3c) could introduce mesopores which act as channels for mass transportation to the active sites in micropores. Table 1 show the highest external surface area and mesoporous volume observed on ZSM-5_{4Na}.

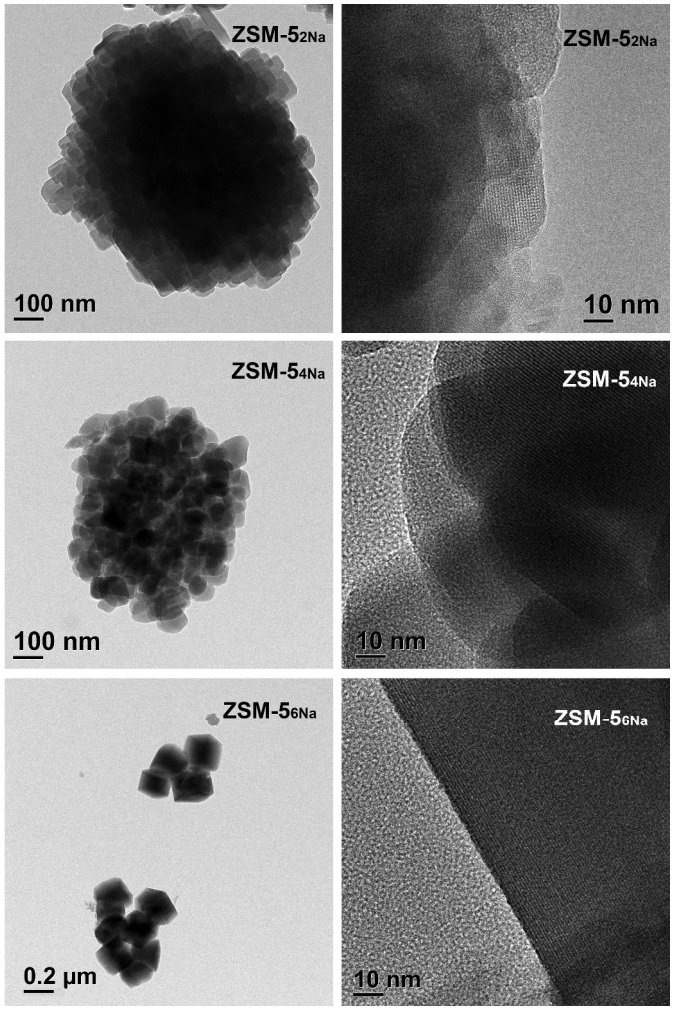

Fig.3 TEM and HRTEM images of ZSM-$5_{x\text{-}Na}$ (x=2, 4, and 6) samples.

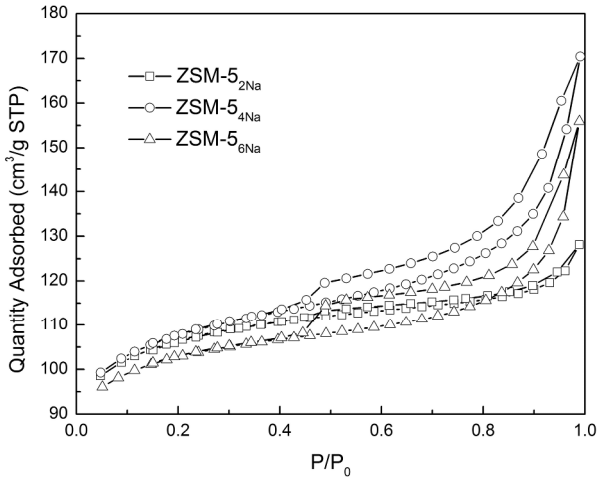

Fig.4 N_2-sorption isotherms of ZSM-$5_{x\text{-}Na}$ (x=2, 4, and 6) samples.

Table 1 Textural parameter of ZSM-$5_{x\text{-}Na}$ (x=2, 4, and 6) samples obtained from N_2-sorption experiments.

Samples	Surface area (m^2/g)			Volume (cm^3/g)		
	BET[a]	External surface[b]	Micropore[b]	Total[c]	Micropore[b]	Mesopore[d]
ZSM-5_{2Na}	349.3	85.1	265.2	0.20	0.13	0.05
ZSM-5_{4Na}	353.9	92.6	261.3	0.26	0.13	0.13
ZSM-5_{6Na}	336.4	75.9	260.5	0.24	0.13	0.10

[a] Value determined by the BET method
[b] Value determined by the t-plot method
[c] Value estimated at P/P_0 of 0.99
[d] Value determined by the BJH desorption cumulative

The N_2-sorption isotherms in Fig.4 illustrate the differences in porosity among ZSM-$5_{x\text{-}Na}$ (x=2, 4, and 6) samples. All curves are identified as Type IV isotherms with Type H3 loops. The H3 loops without limiting adsorption at high P/P_0 (at ~0.5), are attributed to inter-crystalline mesopores in random arrangements without uniform orientation ordering. The different size of hysteresis loops indicates the different volume of hierarchical mesopores in samples. The N_2-sorpotion isotherm of ZSM-5_{6Na} exhibits a broad hysteresis loop, as a result of mesoporous structure among dispersed nanocrystals of MFI zeolite. Table 1 reveals that both mesopore volume and external surface area of hierarchical MFI zeolite sample (ZSM-5_{4Na}) are larger than dispersed MFI nanocrystals sample (ZSM-5_{6Na}). Usually, the reduced particle size results in a higher external surface area. However, the densely aggregation (ZSM-5_{2Na}) make more joint part than loosely aggregation (ZSM-5_{4Na}), which results in lower external surface area and lower mesopore volume. In our view, both the inter-crystalline mesopores among aggregated nanocrystals and the mesoporous structure among dispersed nanocrystals could enhance diffusion ability; but the aggregated zeolite nanocrystals should possess shorter microporous diffusion length because of their reduced primary particle size.

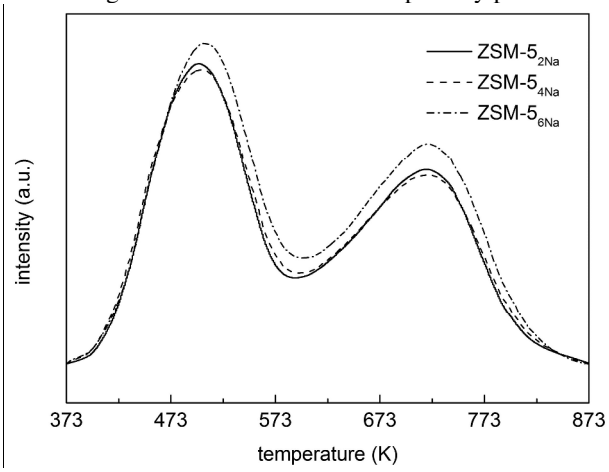

Fig.5 NH_3-TPD profiles of ZSM-$5_{x\text{-}Na}$ (x=2, 4, and 6) samples.

NH_3-TPD measurements (Fig. 5) were carried out to investigate the acidity of the H-ZSM-5 zeolite samples. Each of the profiles is characterized by two desorption peaks in the temperature region of 470–500 and 710–740 K. The desorption peak at low temperature is ascribed to the chemisorption of ammonia molecules on weak acidic sites; and the peak at high temperature is attributed to the desorption on strong Brønsted and Lewis acidic sites. As the same amount of AIP was used in the aluminate-silicate gels for hydrothermal synthesis, all the samples show similar acidity. However, ZSM-5_{6Na} still shows a bit more amount of acidic sites than other two samples. This may be the result of acidic sites in joint parts of zeolite nanocrystals being beyond the accessibility of the ammonia molecules.

3.2 Mechanism of Zeolite Synthesis

The crystallization process of ZSM-5_{4Na} was studied in detail to clarify the mechanism of the present synthetic strategy. The relative crystallinity determined by XRD peak intensity with different crystallization time from 1 to 8 h is shown in Fig.6. A high crystallinity of zeolite requires at least 5 hour crystallization, obviously shorter than the reported crystallization time of hierarchical ZSM-5 usually ranging from 10 h to days in addition to about 20 h pre-crystallization/pre-seeding time. [21-23] It should be noticed that the ZSM-5 zeolites here were prepared by a simple and rapid one-step hydrothermal synthesis with high solid/liquid ratio. This means that a high super-saturation because of the solid/liquid ratio here acts as the drive force of zeolite crystallization[24-26] and a key factor for the formation of zeolite nanocrystals[16]. Moreover, the high solid/liquid ratio in our route results in high super-saturation which mainly contributes to the rapid synthesis of nanocrystals aggregates. Thus, our strategy becomes significant for the industrial application because of its high efficiency and low energy cost.

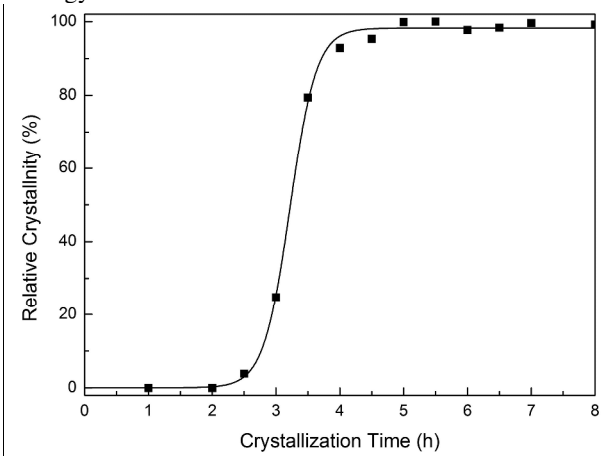

Fig.6 Crystallization curve of the ZSM-5_{8Na} sample.

Fig.7 shows the SEM images of ZSM-5_{4Na} zeolite with different crystallization time. Fig 7a shows the images of non-degradated silica gel after 1 h crystallization, the original silica exhibited large spheres with size of about 40 - 90 μm. After 1.5

h crystallization (Fig.7b), some degradation of the silica sphere was observed through the cracks. Figs. 7c-7f show the partial degradated silica gel after 3 h crystallization at which the crystallization of zeolite started to begin (Fig.6). After 3 h, the partial degradated silica gel remained the morphology of the original silica gel (Fig.7c). For the gel with high super-saturation, the silica gel could not degrade immediately, and then the consumption of degradated silica gel would impel further degradation of silica gel (Fig.7d). Fig 7d shows the interface between degradated part and non-degradated part, the degradated part exhibits a porous morphology. The degradated silica gel exhibits aggregates of amorphous silica of irregular shape (Fig.7e and Fig.7f). Fig 7g and Fig, 7h show the resultant hierarchical MFI zeolite. For Fig 7g, there is an aggregate of hierarchical zeolite, which remains the morphology of the original silica gel. Moreover, the size of zeolite aggregates shown in Fig 7h and the size of degradated silica gel shown in Fig 7e and 7f are particularly in the same range. And no dispersed MFI zeolite nanocrystal could be observed in any crystallization period. These data together show that the conversion from the silica gel to zeolite crystals should be an in-situ conversion taking place in/on the solid phase of silica.

Lasersizer was also introduced to give more direct size information of all crystals and amorphous material in mixture of solid and solution. The sample mixture was completely collected without filtration avoiding the influence of possible agglomeration occurred during the filtrating process. Table 2 indicates that all the particles are larger than 300 nm in all samples obtained at different crystallization time. The d(0.5) decreases (Table 2) as the crystallinity increases (Fig. 6) mostly due to the condensation of silica species during zeolite crystallization. The particles with diameter of 3-100 μm (Table 2) should be ascribed to the mixtures of non-degradated silica gel and MFI zeolites based on size shown in Fig.7. The percentage of these particles did not drop to the minimum level before zeolite crystallization, but decreased as the crystallinity increase. These data together with SEM results suggest that there was no dispersed nanocrystal formed during hierarchical MFI zeolite crystallization, and the zeolite aggregates were not formed through aggregating process of nanocrystals. Instead, the aggregates were generated in-situ converting the silica gel, in which the degradation of silica gel takes place before zeolite crystallization and also simultaneously as the crystallization consumes the degradated silica gel. Thus the size of aggregates could be controlled by adjusting the size of degradated silica gel with different synthesis recipe.

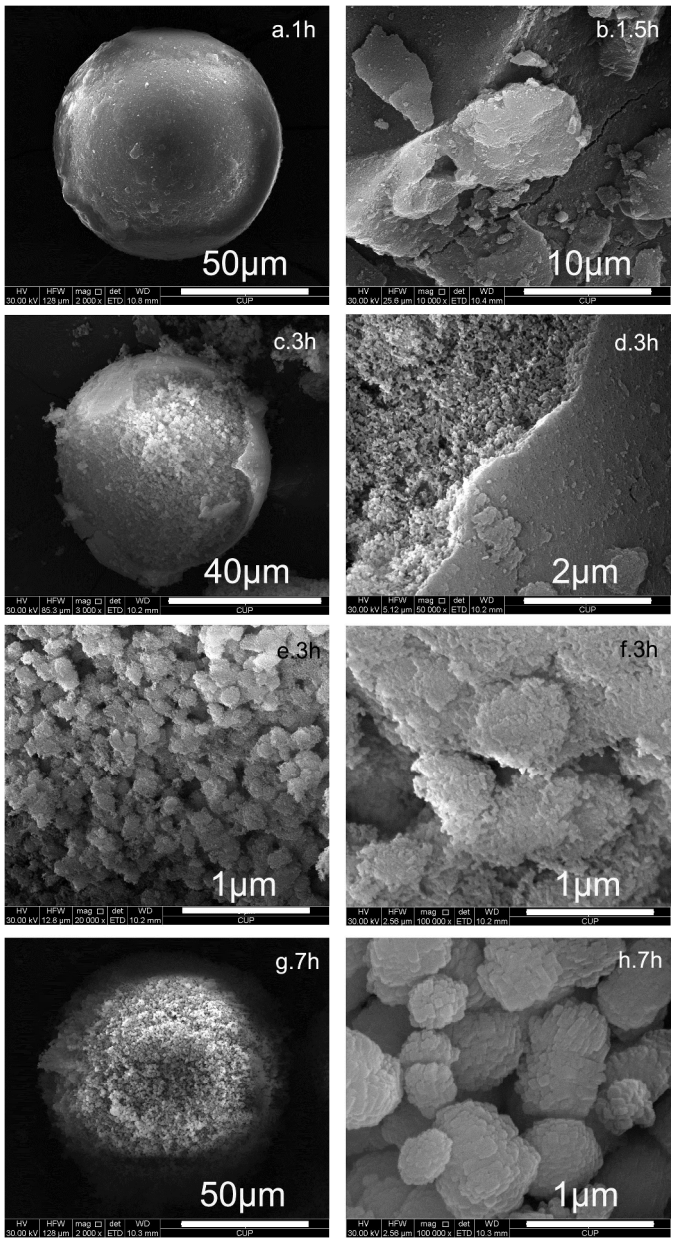

Fig.7 The SEM images of the intermediates and product of the ZSM-5_{4Na} at different crystallization time.

Table 2 the size distribution of mixtures of the intermediates and product of ZSM-5_{4Na} at different crystallization time.

Samples	d(0.5)/ μm	0.02-0.3μm/%	0.3-3μm/%	3-100μm/%
2.5h	1.561	0	78.6	22.4
3.5h	1.377	0	82.7	17.3
4.5h	1.365	0	84.9	15.1
5.5h	1.352	0	86.5	13.5

Section 3.1 shows the feasible control of the primary particle size of MFI zeolite crystal by changing NaBr concentrations in aluminate-silicate gels. It is well known that Na cations play an important role in crystal growth of MFI type zeolite, and the increased amount of Na cations could promote the crystal growth rate.[27] Also, the ionic strength acts an important role of the size and morphology of zeolite. Here, we studied the effect of anions on the zeolite morphology, and a series of ZSM-5_{4Na} zeolites with different anions （Na_2SO_4, NaCl, Na_2CO_3 and NaOH instead of NaBr）were studied. The pH of the solution increases from 14.2 to 14.4 ($Na_2SO_4 \approx$ NaCl<Na_2CO_3<NaOH). The SEM images of Fig.8 show that all samples exhibit aggregates of MFI nanocrystals. Clearly, the morphology of nanocrystals and the size of bulk aggregates (Fig. 8) are in slightly different from the sample using NaBr, the aggregates size decreases as the pH increases. These data suggest little change of aggregation behaviour with different anions, but different oriented zeolite crystal growth with different anions. And Thus, Fig. 2 and Fig. 8 suggest that an appropriate Na cation concentration and pH are the key factors in controlling the sizes and morphologies of the inter-crystalline mesoporous hierarchical MFI zeolite synthesis. Meanwhile, it should be noticed that the tetrapropyl ammonium bromide (TPABr) could be used coupled with NaOH to replace TPAOH as the template for reducing the cost of synthesis.

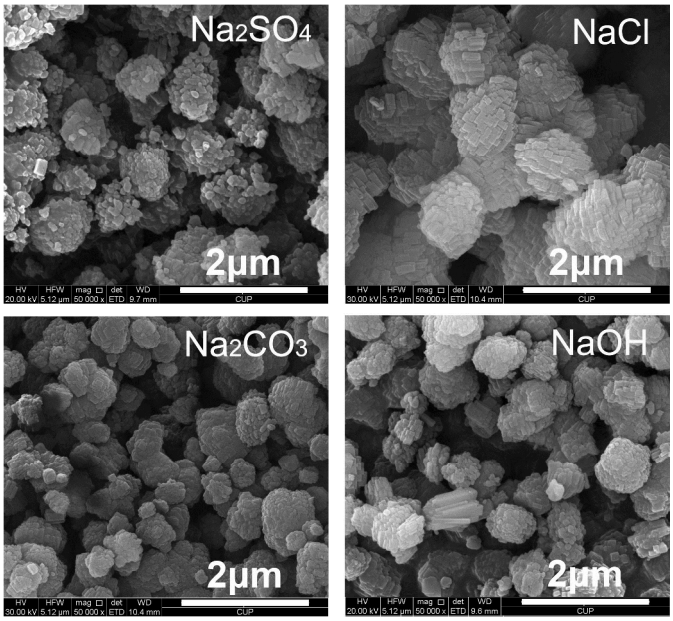

Fig.8 SEM images of ZSM-5_{4Na} samples prepared with different type of sodium salts.

Fig.9 summarizes the facile route of the formation of hierarchical MFI zeolite. Aggregates of nanocrystals are generated by the synchronization of silica gel degradation of and zeolite crystallization. Here, a alkaline solution with high pH value (>14) was required for zeolite synthesis, suggesting the formation of aluminates from AIP. On the other hand, in the mixture with the high solid/liquid ratios, the silica gel dissolved partly into silicate and the other degradated in alkaline solution. The degradated silica gel generated an irregular morphology with many mesopores/macropores accessible to TPA templates and aluminate species with high concentrations due to the high solid/liquid ratio, which generated a new interface between solid and liquid phase with a high super-saturation of amorphous silicate. Then, the nucleation and crystallisation take place in both inside and outside of degradated silica gels. A high solid/liquid ratio in hydrothermal synthesis results in high TPA^+ concentration and then induces a burst in nucleation[28]. A relatively low Na concentration restrains the crystal growth rate and consumption rate of degradated silica gel. As a result, lots of nanocrystals are formed and originally connected with others by consuming the same degradated silica gel particle. Thus the aggregates of nanocrystals are formed without an intermediate state of dispersed nanocrystals or nano-sized zeolite precursors reported in synthesis from clear solution. The morphology of degradated silica gel as well as the size of zeolite aggregates is determined by Na cation concentration and pH of mixture. A higher Na cation concentration could result in a larger size of degradated silica gel and higher crystal growth rate, which hinder the formation of nanocrystals aggregates. As the crystallization consumes the degradated silica gel, the remaining silica gel degradate simultaneously. In this process, the degradation of silica gel and the crystallization of degradated silica gel are both in-situ conversions, so the morphology of the original silica gel and the degradated silica gel are both remained.

Our strategy for the facile synthesis of hierarchical MFI zeolite synthesis could be used in a wide range from a low Si/Al ratio of 40 (ZSM-5 zeolite) to infinite (i.e. Silicate-1 zeolite). This route of high solid/liquid ratio synthesis could be also used for BEA type and EUO type hierarchical zeolites preparation. And it should be noticed that different Na cation concentrations should be used while high Si/Al ratio zeolite crystal growth rate is higher. Moreover, the one-step process requires neither pre-crystallization/pre-seeding procedure nor steam-assisted conversion, and the crystallization time is fairly short, so it is convenient for large-scale production.

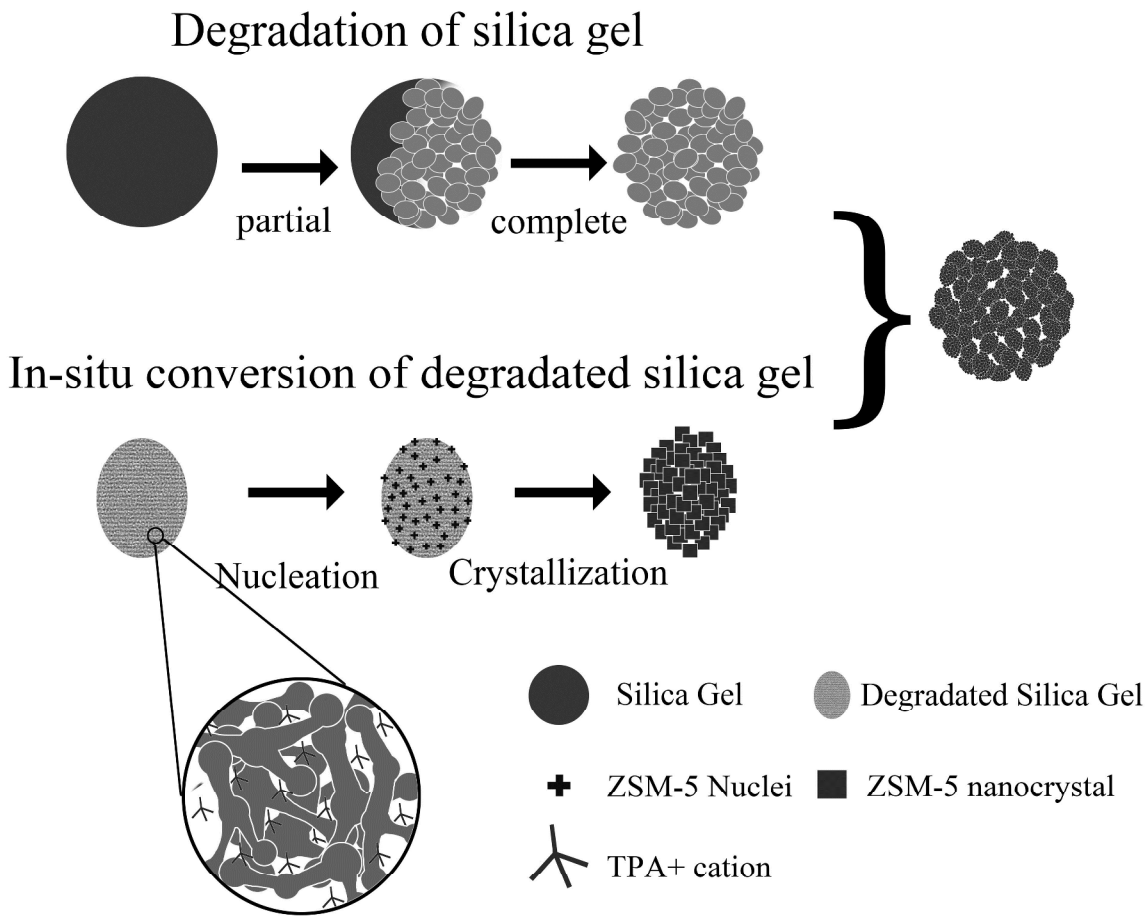

Fig.9 The proposed route for the formation of hierarchical MFI aggregates of nanocrystals.

3.3 Catalytic Performance

Light olefins (ethene and propene) have been mainly manufactured through a naphtha thermal cracking, which requires a high reaction temperature. Thus, the catalytic cracking with a high efficient catalyst is regarded to be an economic route to obtain light olefins from naphtha and attracted much attention. However, the lifetime of catalyst is strongly affected by coking during the cracking reaction, in which the coke fouls the surface of zeolites and blocks the micropores. MFI zeolite has been recognized as a prime candidate as the practical cracking catalyst because of its high thermal and hydrothermal stabilities and its considerable resistance to deactivation by coking. [29,30] Here, ZSM-5_{2Na}, ZSM-5_{4Na}, and ZSM-5_{6Na} zeolite samples were tested in catalytic cracking of n-hexane as a model reaction.

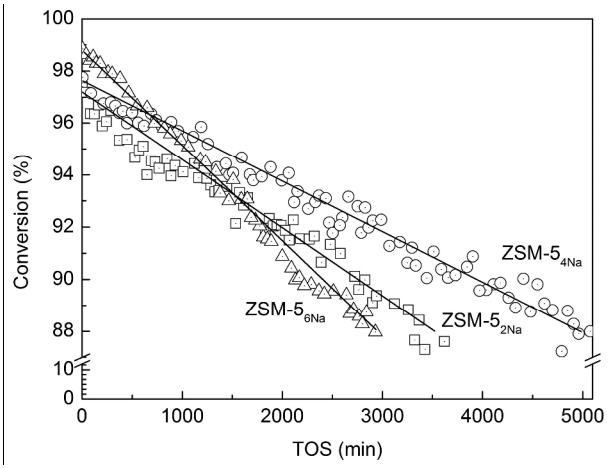

Fig.10 The conversion of n-hexane cracking over ZSM-$5_{x\text{-}Na}$ (x=2, 4, and 6) samples.

The catalytic cracking reactions were examined in a fixed-bed reactor under identical reaction condition (reaction temperature: 900 K; WHSV: 8 h^{-1}). The initial conversion was intentionally controlled above 95% and below 100%. Changes in the n-hexane conversion over different ZSM-5 samples are

shown in Fig.10. The initial conversion of n-hexane was almost the same (approximately 98%), and then gradually decreased with time on stream (TOS). The conversion on ZSM-5_{4Na} sample decreased to approximately 88% within 5000 min. In contrast, a faster decrease to approximately 88% was observed on ZSM-5_{2Na} within 3000 min and ZSM-5_{6Na} within 3600 min, respectively.

The main product selectivities of n-hexane catalytic cracking versus n-hexane conversion of the different samples were shown in Fig.11. No distinguished difference in the main product selectivities is observed among the tested samples, suggesting no remarkable impact of crystal size ranged from 40 nm to 300 nm on the selectivity of n-hexane cracking.

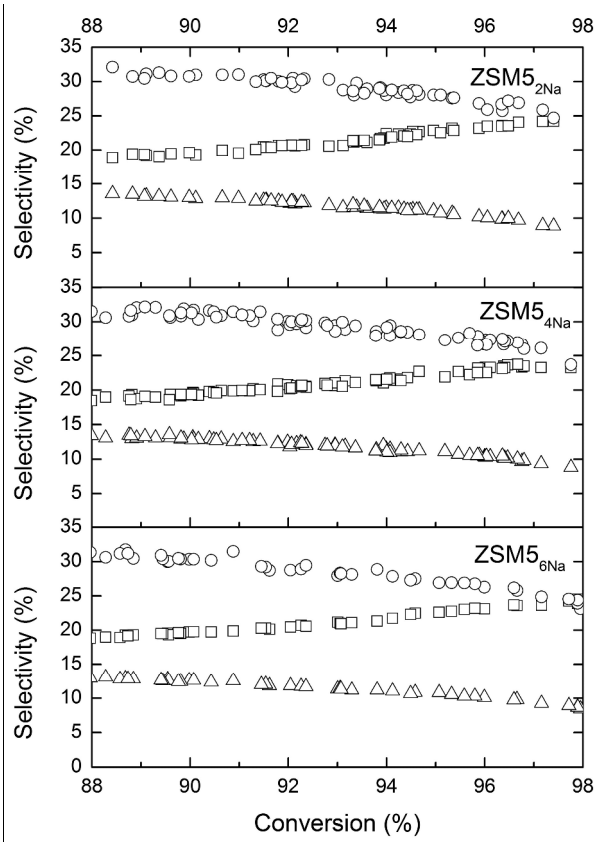

Fig.11 Ethene (□), propene (○) and butene (△) selectivities of n-hexane cracking over the ZSM-$5_{x\text{-}Na}$ (x=2, 4, and 6) samples.

The coke amount of the deactivated samples at the same conversion of approximately 88% was determined by thermogravimetric analyses (Fig. S1). The mass loss above 673K was considered to be the combustion of cokes, and the calculated amount of cokes on ZSM-5_{2Na}, ZSM-5_{4Na} and ZSM-5_{6Na} samples were 8.0 wt.%, 11.5 wt.% and 7.4 wt.% respectively, which has a good consistency with the BET results (Table 1). A large external surface area suggests an increase in the number of micropore entrances and then could retard deactivation resulted from pore blocking. Large mesopore volume could enhance the coke capacity of catalyst. The ZSM-5_{4Na} sample showed much longer lifetime because of its enhanced external surface area and mesopore volume. The average coke formation rates calculated as the amount of cokes divided by TOS were 0.13 wt. %/h, 0.14 wt. %/h and 0.15 wt.%/h on ZSM-5_{2Na}, ZSM-5_{4Na} and ZSM-5_{6Na} respectively, which has a good consistency with the primary particle size of zeolites. ZSM-5_{2Na} sample shows lowest coke formation rate among the tested samples. This may suggest that reduction in diffusion path length could provide low coke formation rate.

Here the inter-crystalline mesoporous hierarchical zeolite (ZSM-5_{4Na}) aggregates show the similar light olefin selectivity but enhanced catalytic lifetime in n-hexane cracking comparing to the highly dispersed zeolite (ZSM-5_{6Na}) nanocrystals. In fact, our inter-crystalline mesoporous hierarchical ZSM-5 zeolites could also promoted both selectivity and lifetime of catalyst in other reactions (i.e., methanol to propylene reaction, Fig. S2 and Table S1). Furthermore, the advantage of facile synthesis and easy separation of the hierarchical ZSM-5_{6Na} zeolite aggregates make an economic merit in potential industrial production. We have already completed 50L-level pilot test of hierarchical MFI zeolite production. Thus, the present synthesis strategy can provide a potential catalyst for catalytic cracking.

4. Conclusions

Here, we report a facile route for the synthesis of hierarchical MFI zeolite via one-step hydrothermal crystallization by in-situ converting solid silica gel to zeolite nanocrystals. The aggregates of MFI zeolite nanocrystals are formed in the synchronization of silica gel degradation and zeolite crystallization. Hierarchical MFI zeolite with controllable inter-crystalline mesopores had been achieved by changing the sodium concentration in aluminate-silicate gels for zeolite synthesis. The resultant hierarchical MFI zeolite aggregates possessed large external surface area and mesopore volume, providing reduced diffusion path length and extra mesopore channels for reactant and product. Compared with highly dispersed MFI zeolite nanocrystals catalyst, a manifest rise (to ~2-fold) in the catalyst lifetime was achieved on the aggregate catalyst in the catalytic cracking of n-hexane. Meanwhile, the present synthetic route offers rapid and simple synthesis procedures which are economic and practical in industrial production. Furthermore, this route with high solid/liquid ratio in aluminate-silicate gels could be also used for the preparation of Silicate-1, BEA and EUO hierarchical zeolites by using solid silica source.

Acknowledgements

The authors acknowledge the Science Foundation of China University of Petroleum-Beijing (YJRC-2013-38), the National Natural Science Foundation of China (21206192), the Doctoral Program of Higher Education of China (20120007120010), and State Key Development Program for Basic Research of China (2012CB215002) for the financial support of this work.

Notes and references

State Key Laboratory of Heavy Oil Processing, Key Laboratory of Catalysis of CNPC, China University of Petroleum, Beijing 102249, China
E-mail: zhijiewu@cup.edu.cn; doutao@cup.edu.cn;
Tel：86-10-89733066；Fax：86-10-89734979

Electronic Supplementary Information (ESI) available: TG curves of deactivated ZSM-$5_{x\text{-}Na}$ (x=2, 4, and 6) samples at the same conversion of approximately 88% in cracking of n-hexane. Catalytic performance of methanol to propylene over hierarchical ZSM-5 zeolite and ZSM-5 nanocrystals.

1 A. Corma, *Chem. Rev.*, 1997, **97**, 2373.
2 C. S. Cundy and P. A. Cox, *Chem. Rev.*, 2003, **103**, 663.
3 N.Y. Chen, W.E. Garwood and F.G. Dwyer, *Shape Selective Catalysis in Industrial Applications*, Marcel Dekker Inc., New York, 1996.
4 B. Li, B. Sun, X. Qian, W. Li, Z. Wu, Z. Sun, M. Qiao, M. Duke and D. Zhao, *J. Am. Chem. Soc.*, 2013, **135**, 1181.
5 N. Viswanadham, J.K. Gupta, G. Murali Dhar and M.O. Garg, *Energy Fuels*, 2006, **20**, 1806.
6 T. Teruoki, K. Hiroki, N. Yuta, M. Takao, *Catal. Surv. Asia,* 2012, **16**, 148.
7 Y. Tao, H. Kanoh and K. Kaneko, *J. Am. Chem. Soc.*, 2003, **125**, 6044.
8 C. J. H. Jacobsen, C. Madsen, J. Houzvicka, I. Schmidt and A. Carlsson, *J. Am. Chem. Soc.*, 2000, **122**, 7116.
9 H. Xu, Y. Zhang, H. Wu, Y. Liu, X. Li, J. Jiang, M. He and P. Wu, *J. Catal.*, 2011, **281**, 263.
10 S. Mitchell, N. L. Michels, K. Kunze and J. Pérez-Ramírez, *Nat. Chem.*, 2012, **4(10)**, 825.
11 J. C. Groen, T. Sano, J. A. Moulijn and J. Pérez-Ramírez, *J. Catal.*, 2007, **251**, 21.
12 B. Li, Z. Hu, B. Kong, J. Wang, W. Li, Z. Sun, X. Qian, Y. Yang, W. Shen, H. Xu and D. Zhao, *Chem. Sci.*, 2014, **5**, 1565.
13 L. Wang, C. Yin, Zh. Shan, S. Liu, Y. Du and F.-Sh. Xiao, *Colloids Surf. A*, 2009, **340**, 126.
14 M. Yu. Kustova, S. B. Rasmussen, A. L. Kustov and C. H. Christensen, *Appl. Catal. B*, 2006, **67**, 60.
15 X. Wang, G. Li, W. Wang, C. Jin and Y. Chen, *Microporous Mesoporous Mater.*, 2011, **142**, 494.
16 L. Tosheva and V. P. Valtchev, *Chem. Mater.*, 2005, **17**, 2494.
17 A. Petushkov, G. Merilis and S. C. Larsen, *Microporous Mesoporous Mater.*, 2011, **143**, 97; A. Petushkov, S. Yoon and S. C. Larsen, *Microporous Mesoporous Mater.*, 2011, **137**, 92.
18 T. Xue, L. Chen, Y. M. Wang and M. Y. He, *Microporous Mesoporous Mater.*, 2012, **156**, 97.
19 M. Sun, L. Chen, X. Li, Y. Yang, Y. Ouyang, W. Geng, Y. Li, X. Yang and B. Su, *Microporous Mesoporous Mater.*, 2013, **182**, 122.
20 M. S. Holm, E. Taarning, K. Egeblad and C. H. Christensen, *Catal. Today.*, 2011, **168(1)**, 3.
21 D. P. Serrano, J. Aguado, J. M. Escola, J. M. Rodríguez and A. Peral, *Chem. Mater.*, 2006, **18**, 2462; D. P. Serrano, J. Aguado, G. Morales, J. M. Rodríguez, A. Peral, M. Thommes, J. D. Epping and B. F. Chmelka, *Chem. Mater.*, 2009, **21**, 641; D. P. Serrano, J. Aguado, J. M. Escola, J. M. Rodríguez and A. Peral, *J. Mater. Chem.*, 2008, **18**, 4210.
22 C. Li, Y. Wang, B. Shi, J. Ren, X. Liu, Y. Wang, Y. Guo, Y. Guo and G. Lu, *Microporous Mesoporous Mater.*, 2009, **117**, 104.
23 K. Möller, B. Yilmaz, R. M. Jacubinas, U. Müller and T. Bein, *J. Am. Chem. Soc.*, 2011, **133**, 5284.
24 I. V. Markov, *Crystal Growth for Beginners: Fundamentals of Nucleation, Crystal Growth and Epitaxy*, World Scientific Pub. Co. Inc., 2003.
25 J. Cejka, A. Corma and S. Zones, *Zeolites and Catalysis: Synthesis, Reactions and Applications*, Wiley-VCH, 2010.
26 R. M. Barrer, *Zeolites: Their Nucleation and Growth (in Zeolite Synthesis, Chapter 2)*, ACS Symposium Series, Vol. 398, 1989, pp11-27.
27 E.G. Derouane and Z. Gabelica, *J. Solid State Chem.*, 1986, **64**, 296; Z. Gabelica, N. Blom and E.G. Derouane, *J. Solid State Chem.*, 1986, **64**, 296.
28 O.A. Fouad, R.M. Mohamed, M.S. Hassan and I.A. Ibrahim, *Catal. Today.*, 2006, **116**, 82.
29 H. Mochizuki, T. Yokoi, H. Imai, R. Watanabe, S. Namba, J. N. Kondo and T. Tatsumi, *Microporous Mesoporous Mater.*, 2011, **145**, 165.
30 H. Konno, T. Tago, Y. Nakasaka, R. Ohnaka, J. Nishimura and T. Masuda, *Microporous Mesoporous Mater.*, 2013, **175**, 25.

